

DEVELOPMENT OF A MINIATURE, MULTICHANNEL, EXTENDED-RANGE FABRY-PEROT FIBER-OPTIC LASER INTERFEROMETER SYSTEM FOR LOW FREQUENCY SI-TRACEABLE DISPLACEMENT MEASUREMENT

Bartosz K. Nowakowski¹, Douglas T. Smith¹, Stuart T. Smith²,
¹National Institute of Standard and Technology
Gaithersburg, Maryland, USA
²Center for Precision Metrology
University of North Carolina at Charlotte
Charlotte, North Carolina, USA

INTRODUCTION

Laser interferometry has become a staple of SI-traceable displacement measurement techniques. With decreasing cost per channel, miniaturization, and a multitude of commercially available off-the-shelf systems, these systems create ever more attractive applications unheard-of a few years ago. Although significant efforts have been made to shrink the size of the optical components necessary for a fully functioning laser interferometer sensor, most currently available commercial sensors have a sensing element on the order of millimeters or more [1].

The goal of the work presented in this paper, which is based on our previous experience with fiber-based laser interferometer systems [2], was to build a directly SI-traceable laser interferometer displacement sensor with a sensor head no bigger than a single optical fiber diameter (0.125 mm). The sensor was designed and built specifically to serve as the primary displacement and force gauge sensor in an SI-traceable precision nanoindentation platform (PNP) [3]. Significant efforts were made to assure that each component not only performed a needed function, but also contained known uncertainties or a specific methodology to ascertain uncertainty values.

SENSOR DESIGN

The sensor is based on a fiber-optic, homodyne, low finesse, single detector Fabry-Perot (FP) cavity that is set up between a polished surface and the cleaved end of an optical fiber (FIGURE 1). When the cavity length changes, a Fabry-Perot laser interferometer system has an output best described by an Airy function, and is typically used only near a quadrature point, *i.e.*, the mid-point between an interference maximum

and minimum. At or near that point, the intensity-displacement relation is assumed to be linear to within a 1 % error for displacements on the order of 100 nm for wavelengths near 1550 nm, but displacements larger than this cannot be tracked.

To overcome this limitation and extend the working range of our sensor, the laser wavelength (nominally 1550 nm) is continuously modulated sinusoidally at a frequency of $f = 1.2$ kHz, which was chosen based on the upper modulation frequency limit of our rapidly tunable laser (RTL). By sinusoidally modulating the wavelength while cavity length, h , is being changed, the signal measured by the detector has a spectrum consisting of responses at the modulation frequency f and its harmonics. The optimal modulation depth depends on the cavity length, and typically is 0.5 nm (peak-to-peak) for cavities on the order of few mm. Taking a closer look at the f and $2f$ signal intensities, I_f and I_{2f} respectively (FIGURE 2), it can be seen that when the cavity is changing they resemble sine

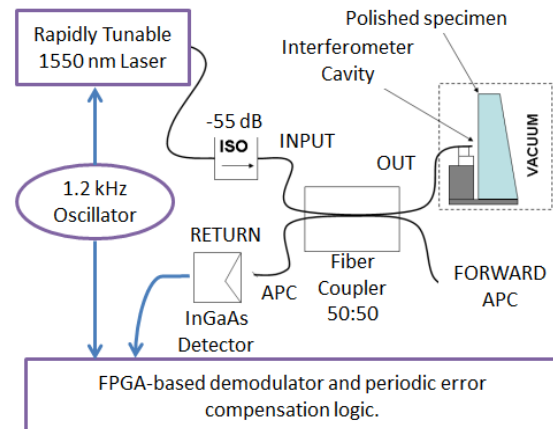


FIGURE 1. Main system components.

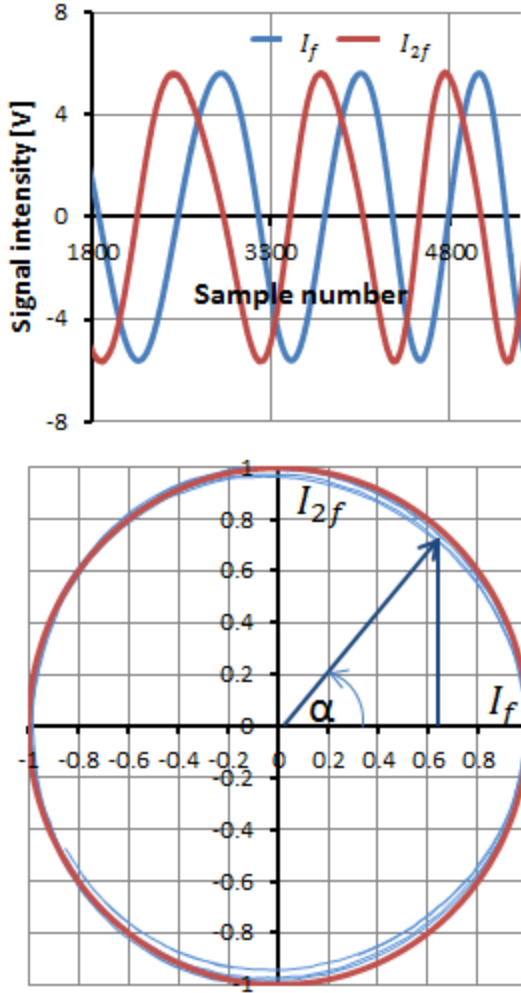


FIGURE 2. (Top) Demodulated signals at f and $2f$ during mirror displacement. (Bottom) f and $2f$ combined into a rotating vector.

and cosine. Those signals can be combined into a rotating vector created between point $(0,0)$ and point (I_f, I_{2f}) . Changes in cavity length caused by motion of the polished surface can then be calculated from:

$$\Delta h = \frac{\lambda}{2} \left(\frac{\alpha}{360} + n \right), \quad \alpha = \arctan \left(\frac{I_{2f}}{I_f} \right),$$

where λ is the wavelength, n is the number of times the vector completes a full revolution, and α is the angle (in degrees) formed between the vector and the horizontal axis. This approach extends the working distance of a laser interferometer to well beyond 25 mm, while still maintaining sub-nanometer resolution.

ERROR COMPENSATION STRATEGIES

Compensation for fringe asymmetry

One inherent problem related to using a FP cavity in this extended mode is the inclusion of periodic errors described by Wilkinson *et al.* [4]. We have developed two methods for reducing these errors: one based on a look-up table created during system operation, and another based on post-processing the data using the model developed in Ref. [4].

Experimental approach to error compensation

In this method, a cavity is continuously swept by an open-loop piezoelectric-based nano-positioner capable of a maximum displacement of approximately $35 \mu\text{m}$. It is generally known that piezoelectric actuators, if operated in voltage-controlled mode, exhibit nonlinear voltage-displacement characteristics. During a $35 \mu\text{m}$ cavity sweep with 1550 nm laser wavelength, the rotating vector completes a maximum of 45 full revolutions. Because all these data can be stored and overlapped, they

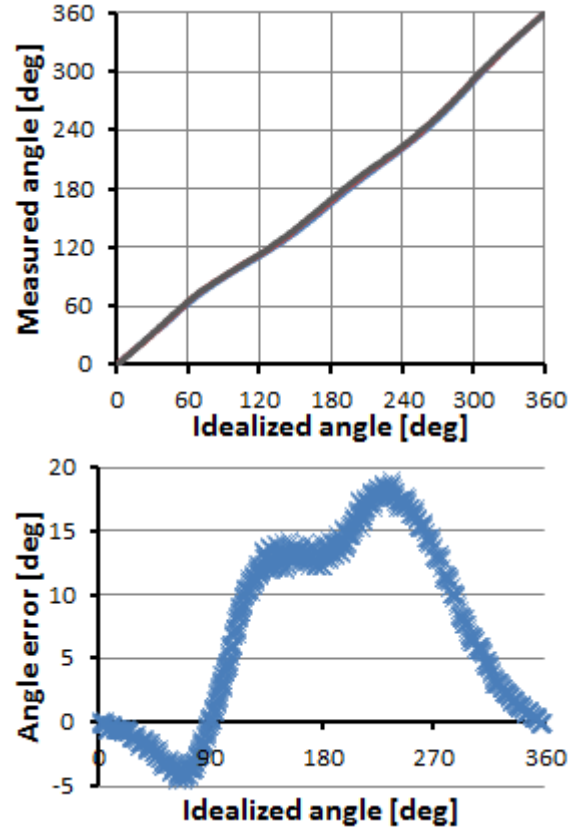


FIGURE 3. Residual periodic error mapped during laser initialization (10 cycles overlapped).

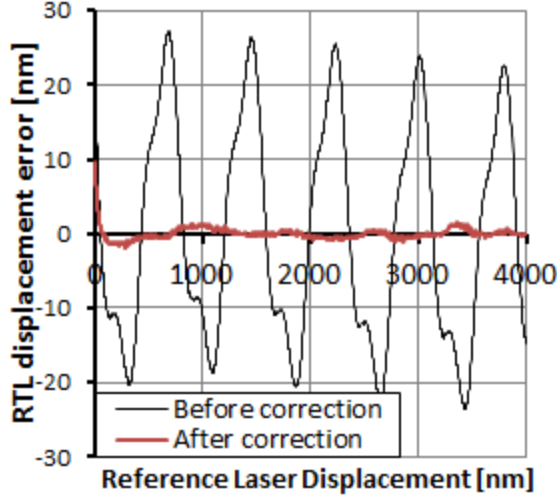


FIGURE 4. Residual periodic error before and after correction, relative to a reference laser.

can be averaged in post-processing to reveal cyclic nonlinearities, as shown in FIGURE 3. In this figure (top), the idealized angle is reconstructed; that is, the angle that the vector should have if no nonlinearities existed, is plotted against the actual measured angle. In the bottom figure, multiple overlapped cycles are presented with angular errors extracted. A bicubic spline function is then used to fit the data to average all overlapping cycles into one monotonic data set. These data form a base for creating a 7200 point lookup table with linear interpolation used in between points.

By using this method alone, it was possible to reduce the amplitude of the periodic errors from approximately 50 nm down to the single-nanometer level (FIGURE 4).

Analytical approach to error compensation

This section provides a brief overview of an ongoing study to evaluate a theoretical model of this interferometer implementation. Assuming an approximately Gaussian beam profile, Nemoto and Nakimoto [5] produced a theoretical model for predicting beam coupling between two fibers. Wilkinson and Pratt [4] adapted this to model field reflectance of the fiber and mirror interferometer. In this paper, they develop the following equation to model the coupling of each successive reflection of the cavity. In this model the coupling can be expressed in terms of the n^{th} reflection (this should not be confused with the refractive index of the cavity n_c). Hence the coupling C_n for the n^{th} reflection is given by [4]

$$C_n = \Delta e^{i\beta_n} e^{i\Theta_n}$$

$$\Delta_n = \frac{1}{\sqrt{1+n^2\bar{z}_m^2}} e^{\left[\frac{kz_R(1+5n^2\bar{z}_m^2)}{1+n^2\bar{z}_m^2} n^2\theta_m^2 \right]}$$

$$\Theta_n = -\tan^{-1}(n\bar{z}_m) + \frac{kz_R(3n\bar{z}_m - n^3\bar{z}_m^3)}{1+n^2\bar{z}_m^2} n^2\theta_m^2$$

$$\beta = 2nkz$$

where k is the wave vector in the cavity ($= 2\pi n_c / \lambda$), z_R is the Rayleigh length ($= ks^2$), s is the spot radius, λ is the vacuum wavelength of the illumination source, $\bar{z} = z / z_R$ is the normalized separation of the cavity, $\bar{x} = x / z_R$ is the normalized lateral (or transverse) shift of the reflecting beam and θ_m is the angular misalignment between the two surfaces of the cavity. Summing the coupling of the beam into the fiber for each reflection, the resultant complex value will provide the field reflectance of the cavity.

Having calculated the coupling coefficient for each reflection of the beam, the total field reflectivity, r , of the cavity is computed from the complex sum of reflections [4]:

$$r = r_o C_o + \frac{t_o^2}{r_o} \sum_{n=1}^{\infty} (r_m r_o)^n C_n e^{-i\pi}$$

where r_m and r_o represent the field reflectivity of the mirror and fiber end-face and t_o the transmitted field. The net result of this analysis is a complex number representing the magnitude and phase of the Fabry-Perot mirror. Squaring the field reflectivity produces the intensity reflectance corresponding to the voltage output of the detector.

In order to model experimental f and $2f$ responses like those shown in FIGURE 2, the first and second modulation harmonics are calculated and compared with the real and imaginary components of the cavity with a glass reflecting surface, FIGURE 5. From this model, a cavity misalignment of 47.7 mrad, minimum separation of 2.0056 mm and field reflectivity of 0.2011 were derived from the fit coefficients.

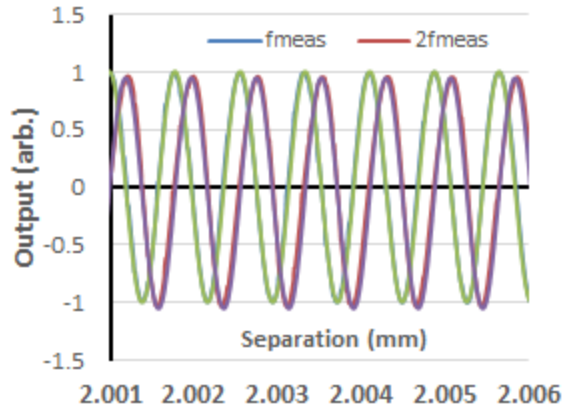


FIGURE 5: Plots of the first two harmonics of the modulation signals from the interferometer with fits of the real (green) and imaginary (purple) response of the theoretical model overlaid.

As of this writing, the theoretical model above deviates from reflectance measurement of the FP cavity at around the 1% level. While further analysis may reduce these deviations, it is likely that the discrepancies are due to differences between the physics of the model and that of the experimental apparatus and measurement methods. Possible error sources include: non sinusoidal time modulation of the source beam, the normalization methodology used to extract phase from the quadrature signal, the non-sinusoidal nature of the FP cavity reflectance, errors with the assumed Gaussian beam profile, and errors associated with the assumption that the spot size from which the Rayleigh length is calculated is the same as the fiber diameter.

It is mainly because of these uncertainties that a more robust approach based on renormalization and look-up tables is being pursued, an approach also adopted in [1].

Amplitude normalization technique and offset removal

Other sources of periodic errors include differences in f and $2f$ amplitudes, as well as minute DC voltage offsets present on signals. Since basic trigonometry is used to compute angle from f and $2f$ intensities, it is assumed that their corresponding amplitudes are equal, and the rotating vector forms a perfect circle centered at the point (0,0). Any deviation from that creates periodic errors.

Amplitudes of both f and $2f$ depend strongly on laser wavelength modulation depth, the optimal

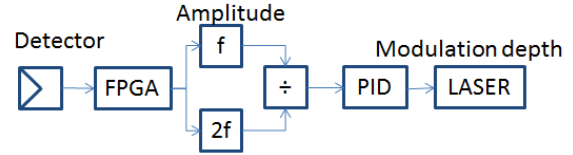


FIGURE 6. Mechanism of reducing periodic errors due to f and $2f$ amplitude difference.

amplitude of which is dependent on laser cavity length: the longer the cavity, the smaller the modulation depth required.

In order to maintain a constant ratio of f and $2f$ amplitudes, a closed-loop proportional-integral-derivative (PID) system was incorporated; it is presented schematically in FIGURE 6. The signal from a detector is separated into f and $2f$ components using a lock-in amplifier implemented with field-programmable-gate-array (FPGA) methods. Amplitudes and residual offsets of the f and $2f$ signals are then measured individually for every interference cycle. Offsets are then removed by subtracting the measured values from corresponding f and $2f$ signals. The amplitude ratio of f and $2f$ is sent to the PID controller, which changes wavelength modulation depth to keep the ratio at unity.

ABSOLUTE CAVITY LENGTH MEASUREMENT

Because the laser wavelength can be easily changed by applying an input voltage to the laser control module, the absolute cavity length can be measured by sweeping wavelength and counting the number of times the interferometer signal reaches its peak. Knowing the wavelength at the first maximum (λ_1) and last (λ_2) and the number of interference cycles (m) in between, the absolute cavity length (h) can be computed from the following equation:

$$h = \frac{m}{2} \left(\frac{\lambda_1 \cdot \lambda_2}{\lambda_2 - \lambda_1} \right).$$

The biggest contributor to uncertainty in this cavity length determination method is how accurately wavelengths at interference maxima can be determined.

SENSOR PERFORMANCE

Sensor stability and noise

There are various methods of stabilizing the laser wavelength in interferometry applications.

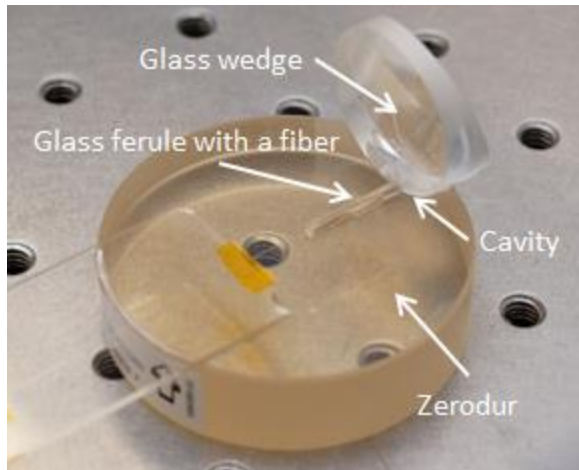


FIGURE 7. Stable cavity assembly for laser stability test.

Many systems have been developed using a reference gas absorption cell or a reference Fabry-Perot cavity. In this work, laser stability is achieved by measuring wavelength with an optical spectrum analyzer (OSA). The OSA continuously sends wavelength and modulation depth information through an RS-232 interface to a real-time control module used as a PID controller. This scheme allows low-picometer wavelength stability while maintaining the flexibility to choose the operating wavelength.

In order to test how stable the displacement measurement is in a fully operational instrument deployed in its working environment, a test setup was built (see FIGURE 7). A glass ferrule holding an optical fiber was mounted with a dab of glue to a glass substrate having a very low coefficient of thermal expansion. An optical cavity was formed between a cleaved fiber end and an optically polished glass wedge attached to the substrate. Care was taken to assure that

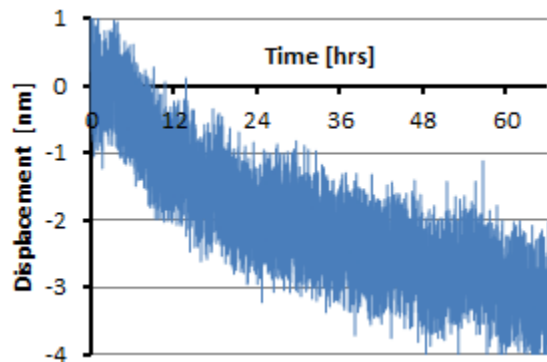


FIGURE 8. Laser stability test over 66 hours (data acquired at a rate of 10 samples per minute).

the metrology loop was as short as feasible. The assembly was then placed in a temperature-controlled chamber capable of maintaining a temperature setpoint to approximately 0.01 °C.

Data obtained during the logging of displacement are shown in FIGURE 8. Data were recorded over 66 h at a rate of 10 samples per minute. The average stability of the sensor during this experiment was measured to be approximately 1 nm per 24 h. The exponentially decaying drift is likely caused by handling the assembly prior to recording data. Higher-frequency variations in displacement are caused primarily by the dynamics of the environmental chamber PID temperature control system.

The noise performance of the system at higher frequencies can be seen in FIGURE 9. Here data were recorded at the rate of 74 Hz. Data obtained follows a normal distribution with 6σ of 0.914 nm and noise amplitude $0.106 \text{ nm}/\sqrt{\text{Hz}}$.

Maximum range for a mirror-polished target

The maximum working range of our system, which uses a source laser power of approximately 5 mW, was determined by moving the cleaved fiber end away from target until accurate nanometer level displacement measurement was no longer possible. The maximum distance was determined to be approximately 25 mm, which is more than adequate for the current application.

Angular misalignment and target roughness

One major advantage of using a bare cleaved fiber is that careful fiber-target alignment using focusing lenses is not required. The maximum possible misalignment at which the

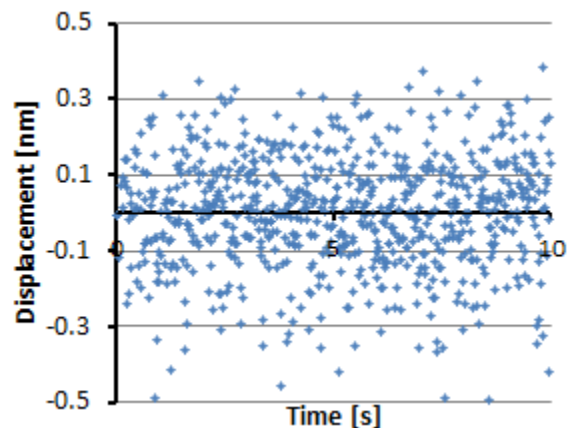


FIGURE 9. Laser system displacement noise measurement.

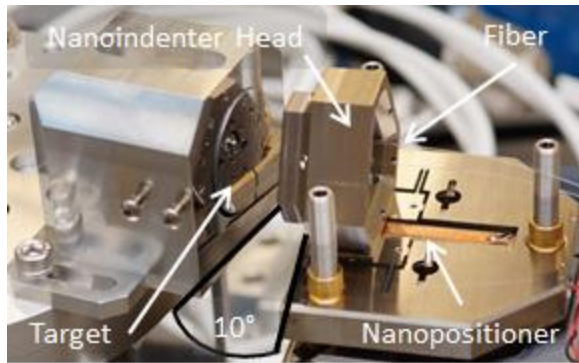


FIGURE 10. Fiber-target misalignment.

interferometer would still work was $\pm 10^\circ$, when tested on an optically polished aluminum target. The setup and misalignment can be seen in FIGURE 10. This feature greatly reduces set-up time and precision required for the fiber-target pair during assembly. Although the system can function with high degrees of misalignment, it is not advised to operate at those limits without careful consideration of the beam path to reduce unwanted uncertainty.

Typical laser interferometer systems require an optically polished target surface to operate properly. To test how our system behaves when the target surface is of significantly poorer optical quality, we used a set of targets made from common nanoindentation specimens. They are presented in FIGURE 11. In order they are: 1) a cured epoxy resin, 2) poly (methyl methacrylate), 3) a polished polycrystalline ceramic, 4) a silicon wafer, and 5) high-density polyethylene.

There was no distinguishable difference between any of those samples and a polished Al mirror in the performance of the system. The interferometer system was stable and the noise level remained at the reference level.

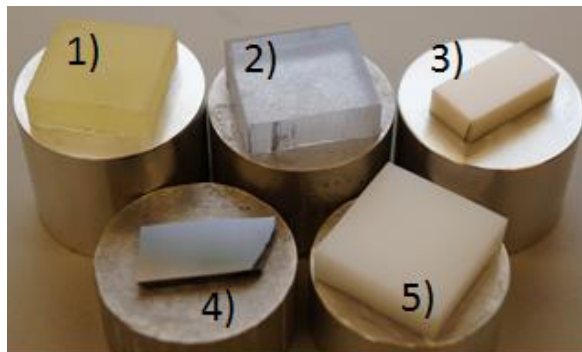


FIGURE 11. A variety of materials that all created functional Fabry-Perot cavities.

CONCLUSION

This paper presents the development of a miniature, multichannel, extended Fabry-Perot fiber-optic laser interferometer system designed for a precision SI-traceable nanoindentation application. The system meets all requirements, achieving sub-nanometer noise levels, high stability, immunity to minute fiber-target misalignments and a surprising level of immunity to surface roughness. Periodic errors can be successfully reduced using the methods described.

DISCLAIMER

Commercial equipment and materials may be identified in order to adequately specify certain procedures. In no case does such identification imply recommendation or endorsement by the National Institute of Standards and Technology, nor does it imply that the materials or equipment identified are necessarily the best available for the purpose.

REFERENCES

- [1] K. Thurner, P.-F. Braun, and K. Karrai, Absolute distance sensing by two laser optical interferometry, *Rev. Sci. Instrum.* 84, 115002 (2013).
- [2] D. T. Smith, J. R. Pratt, and L.P. Howard, A fiber-optic interferometer with subpicometer resolution for dc and low-frequency displacement measurement, *Rev. Sci. Instrum.* 80, 035105 (2009).
- [3] B.K. Nowakowski, D.T. Smith, S.T. Smith, L.F. Correa, and R.F. Cook, Development of a precision nanoindentation platform, *Rev. Sci. Instrum.* 84, 075110 (2013).
- [4] P.R. Wilkinson and J.R. Pratt, Analytical model for low finesse, external cavity, fiber Fabry-Perot interferometers including multiple reflections and angular misalignment, *Applied Optics* 50, p. 4671 (2011).
- [5] S. Nemoto and T. Makimoto, Analysis of splice loss in single-mode fibres using a Gaussian field approximation, *Opt. and Quantum Elec.* 11, 447 (1979).